REGULAR ARTICLES

Renormalization and destruction of $1/\gamma^2$ tori in the standard nontwist map

A. Apte, A. Wurm, and P. J. Morrison
Department of Physics and Institute for Fusion Studies, University of Texas at Austin, Austin, Texas 78712

(Received 31 October 2002; accepted 8 January 2003; published 7 March 2003)

Extending the work of del-Castillo-Negrete, Greene, and Morrison [Physica D **91**, 1 (1996); **100**, 311 (1997)] on the standard nontwist map, the breakup of an invariant torus with winding number equal to the inverse golden mean squared is studied. Improved numerical techniques provide the greater accuracy that is needed for this case. The new results are interpreted within the renormalization group framework by constructing a renormalization operator on the space of commuting map pairs, and by studying the fixed points of the so constructed operator. © *2003 American Institute of Physics.* [DOI: 10.1063/1.1555472]

In recent years, area-preserving maps that violate the twist condition locally in phase space have been the object of interest in several studies in physics and mathematics. These *nontwist* maps show up in a variety of physical models. An important problem from the physics point of view is the understanding of the breakup of invariant tori, which show remarkable resilience in the region where the twist condition is violated, called *shearless tori*. In terms of the physical system modeled, these tori represent transport barriers, and their breakup corresponds to the transition to global chaos. Mathematically, nontwist maps present a challenge since the standard proofs of celebrated theorems in the theory of area-preserving maps rely heavily on the twist condition. In this article, we study the breakup of the shearless torus with winding number $1/\gamma^2$, where γ is the golden mean. This torus serves as a test case for improved techniques we developed. At the point of breakup the shearless torus exhibits universal scaling behavior which leads to a renormalization group interpretation.

I. INTRODUCTION

In this article we consider the *standard nontwist map* (SNM) M, as introduced in Ref. 1:

$$x_{n+1}=x_n+a(1-y_{n+1}^2),$$
$$y_{n+1}=y_n-b\ \sin(2\pi x_n), \tag{1}$$

where $(x,y)\in\mathbb{T}\times\mathbb{R}$, $a\in(0,1)$, and $b\in(-\infty,\infty)$. The map M is *area-preserving* and violates the *twist condition*

$$\frac{\partial x_{i+1}(x_i,y_i)}{\partial y_i}\neq 0, \quad \forall(x_i,y_i), \tag{2}$$

along a curve in phase space, which has been recently called the *nonmonotone curve* (which coincides with the shearless curve when $b=0$).[2] Traditionally, most studies of area-preserving maps have dealt with the *twist* case, but in recent years more and more research has been focused on the nontwist case.

Applications of nontwist maps occur in many fields, for example, the study of magnetic field lines in toroidal plasma devices (see, e.g., Refs. 3 and 4), in celestial mechanics,[5] fluid dynamics[1] and atomic physics.[6] It has been shown[7,8] that nontwist regions appear generically in area-preserving maps that have a tripling bifurcation of an elliptic fixed point. In addition to these applications, the map is quite interesting from a mathematical standpoint because many important theorems in the theory of area-preserving maps assume the validity of the twist condition, e.g., the KAM theorem and the Poincare–Birkhoff theorem. The SNM can serve as a model for the development of new proofs. Up to now, only a few mathematical results exist for nontwist maps (see, e.g., Refs. 2 and 9–11).

We continue the work of del-Castillo-Negrete, Greene and Morrison,[12,13] who studied the breakup of the shearless invariant torus with winding number $1/\gamma$, where $\gamma=(1+\sqrt{5})/2$ is the golden mean. We present the analysis of the breakup of the shearless invariant torus with winding number (in continued fraction representation)

$$\omega=[0,2,1,1,\ldots]=1/\gamma^2. \tag{3}$$

Because this winding number is a noble number (its continued fraction expansion ends with $[1,1,1,\ldots]$), the behavior of the residues of the approximating periodic orbits is expected to be the same as in the $1/\gamma$ case, i.e., we should find the same fixed point of the renormalization group operator with the same unstable eigenvalues that were found in Ref. 13. But, the form of the renormalization group operator, which is defined later in Sec. IV, is different from the $1/\gamma$ case. Also, the region of parameter space we study is different. Additionally, since the periods of approximating periodic

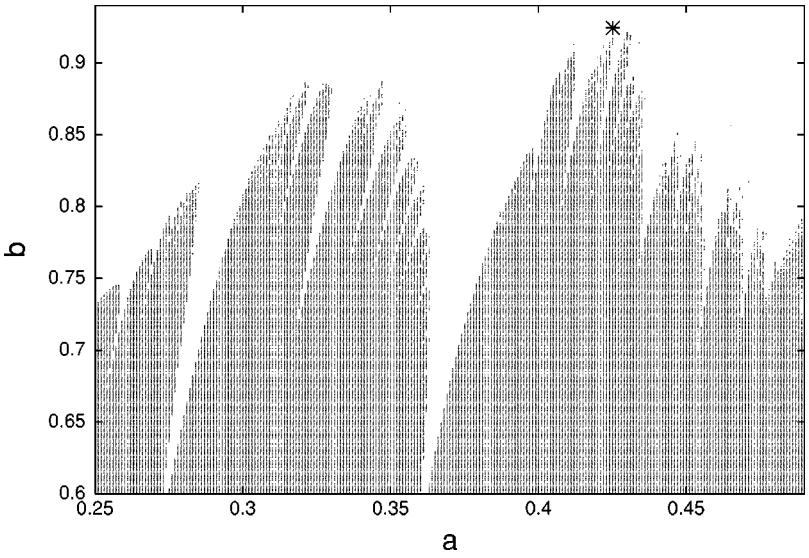

FIG. 1. Parameter space around the critical point (marked by *) of the $\omega=1/\gamma^2$-shearless curve, showing the points for which shearless invariant tori exist.

orbits are bigger than those for the $1/\gamma$ case, the present work serves as a test case for improved numerical techniques described later in Sec. III A.

A different approach, which yields rough parameter values for the breakup of invariant tori, was used by Shinohara and Aizawa in Ref. 14, who showed that a shearless invariant torus crosses the x-axis at two points,[15] $x_A=a/2-\frac{1}{4}$ and $x_B=a/2+\frac{1}{4}$. For a given (a,b), a point on the shearless torus, $(a/2+\frac{1}{4},0)$, is iterated many times (we used 10^6). If the y value stays below a threshold (we used $|y|<0.52$), it is assumed that the shearless curve exists and the point is plotted. Figure 1 depicts our duplication of their procedure.

We see that the critical point for the $1/\gamma^2$ shearless curve (indicated by *) lies on the boundary in Fig. 1. Thus, the boundary points of Fig. 1 represent the *critical function* for the SNM. This is a generalization of the definition of the critical function for the standard twist map (see, e.g., Ref. 16), which has only one parameter, e.g., k. The critical function in the twist case is then defined as $k_c(\omega)$. Here, we have two parameters, but the shearless invariant torus of a given winding number ω exists only for parameter values belonging to a curve $(a,b(a;\omega))$ in the parameter space. Thus, we can define the critical function by the critical points on each of those curves by $(a_c,b(a_c;\omega))$. By finding the critical points for many other winding numbers (both nobles and non-nobles), we hope to find a more accurate critical function curve than the one shown in Fig. 1.

In Sec. II, we review some basic properties of the SNM. The detailed breakup of the shearless invariant torus with winding number $1/\gamma^2$ is presented in Sec. III, which also contains a discussion of the numerical procedures involved. In Sec. IV, we interpret the results within the framework of the renormalization group. Section V contains a summary and some directions of future research.

II. REVIEW OF RESIDUE CRITERION AND STANDARD NONTWIST MAP

In this section, we give a brief review of some basic concepts of the theory of area-preserving maps in the context of the SNM. For a more in-depth discussion the reader is referred to Ref. 12 and references therein.

A. Periodic orbits and residue criterion

Since the pioneering work of Greene,[17] periodic orbits have proven to be very useful for studying the breakup of invariant tori in area-preserving maps. Below are some standard definitions.

An *orbit* of an area-preserving map M is a sequence of points $\{(x_i,y_i)\}$ such that $M(x_i,y_i)=(x_{i+1},y_{i+1})$. The *winding number* ω of an orbit is defined as $\omega=\lim_{i\to\infty}(x_i/i)$ when the limit exists. Here the x-coordinate is "lifted" from $\mathbb{T}$ to $\mathbb{R}$. A *periodic orbit* of period n is a sequence of n points $\{(x_i,y_i)\}_{i=1}^n$, such that $M^n(x_i,y_i)=(x_i+m,y_i)$ for all $i=1,\ldots,n$, and m is an integer. Periodic orbits have rational winding numbers $\omega=m/n$. An *invariant torus* is an orbit with irrational winding number that covers densely a one-dimensional set in phase space. Of particular importance are the invariant tori that wind around the x-domain because, in two-dimensional maps, they act as transport barriers.

The linear stability of a periodic orbit is determined by the value of its *residue*,[17] R, which is defined as $R:=[2-\mathrm{Tr}(L)]/4$. Here, L is the map M^n linearized about the periodic orbit of interest and Tr denotes the trace. If $0<R<1$, the orbit is stable or elliptic; if $R<0$ or $R>1$, it is unstable or hyperbolic; in the degenerate cases $R=0$ and $R=1$, it is parabolic.

Periodic orbits can be used to systematically approximate invariant tori.[17] The method is based on the observation that given a sequence of rational numbers $\{m_i/n_i\}$ whose limit is ω, the sequence of periodic orbits with winding numbers $\{m_i/n_i\}$ approaches the invariant torus with winding number ω in phase space. It is important to find the "best" possible sequence, i.e., the sequence that converges to ω the fastest. The elements of the best possible sequence (see, e.g., Ref. 18) are the convergents that are obtained from successive truncations of the continued fraction expansion of ω.

The *residue criterion*[17] can be stated as follows: Consider an invariant torus with winding number ω. Let $\{m_i/n_i\}$ be the sequence of convergents approximating ω, and R_i the residues of their corresponding periodic orbits.

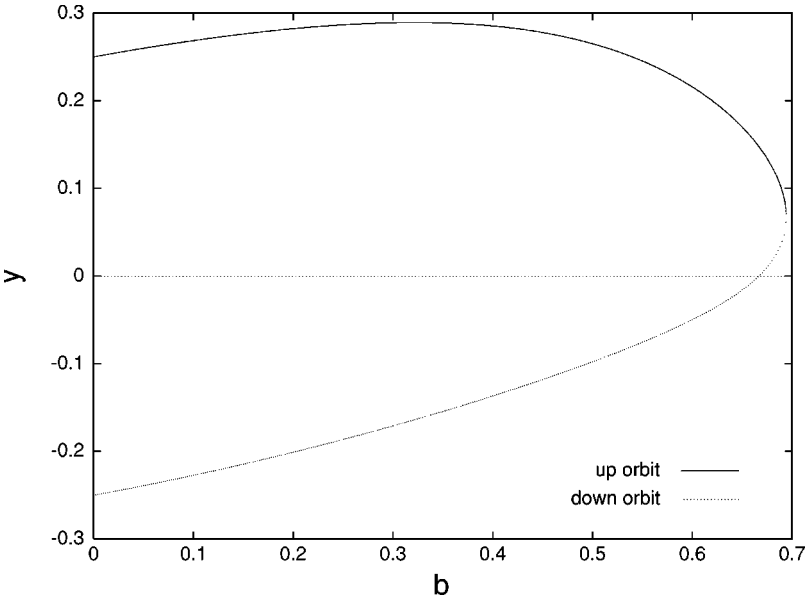

FIG. 2. Plot of behavior of the up and down periodic orbits of winding number 3/8 for increasing b-values at $a=0.4$. The vertical axis shows the y-coordinates of the orbits along s_1.

(1) If $\lim_{i\to\infty}|R_i|=0$, the invariant torus exists.
(2) If $\lim_{i\to\infty}|R_i|=\infty$, the invariant torus is destroyed.
(3) At the boundary in parameter space between those two limits, the invariant torus is at the threshold of destruction and the residues either converge to a constant, nonzero value, or there are convergent subsequences.

This criterion is based on the idea that the destruction of an invariant torus is caused by the destabilization of nearby periodic orbits. The residue criterion has been used successfully in many cases to predict with high precision the threshold for the destruction of invariant tori. Several theorems have been proved that lend mathematical support to the criterion.[19,20]

The numerical search for periodic orbits is difficult because, in principle, it is a two-dimensional root finding problem. However, the task is considerably simplified for *reversible maps*,[17,21] which are maps that can be factored as $M=I_1\circ I_0$, where $I_{0,1}$ are *involution* maps that satisfy $I_1^2=I_0^2=1$. The sets of fixed points of the involution maps, $\Gamma_{0,1}=\{(x,y)|I_{0,1}(x,y)=(x,y)\}$, are one-dimensional sets, called *symmetry lines* of the map. Once we know $\Gamma_{0,1}$, the search for periodic orbits is reduced to a one-dimensional root finding problem, as explained below in Sec. III A 1.

B. Standard nontwist map

The SNM is reversible. The symmetry lines Γ_0, composed of fixed points of I_0, are $s_1=\{(x,y)|x=0\}$ and $s_2=\{(x,y)|x=1/2\}$. The symmetry lines Γ_1, composed of fixed points of I_1 are $s_3=\{(x,y)|x=a(1-y^2)/2\}$ and $s_4=\{(x,y)|x=a(1-y^2)/2+1/2\}$.

A major difference between the standard nontwist map and twist maps is that there are two periodic orbits, if they exist, with the same winding number on each symmetry line. This can be seen easily in the integrable case. For $b=0$, the m/n periodic orbits on the s_1 symmetry line are located at

$$(x,y)=(0,\pm\sqrt{1-(m/n)/a}). \tag{4}$$

We will call the orbit with the bigger (smaller) y-coordinate the *up* (*down*) periodic orbit.

The SNM is also invariant with respect to the transformation

$$T(x,y)=(x+\tfrac{1}{2},-y). \tag{5}$$

The coordinates of the up and down periodic orbits on the symmetry lines s_i, denoted by (x_{ui},y_{ui}) and (x_{di},y_{di}), respectively, are related by this symmetry as follows:

$$\begin{aligned}&(x_{d2},y_{d2})=T((x_{u1},y_{u1})),\quad (x_{u2},y_{u2})=T((x_{d1},y_{d1})),\\&(x_{d4},y_{d4})=T((x_{u3},y_{u3})),\quad (x_{u4},y_{u4})=T((x_{d3},y_{d3})).\end{aligned} \tag{6}$$

Therefore, it is actually enough to compute periodic orbits on s_1 and s_3, since the orbits along the other symmetry lines can be obtained from (6).

C. Periodic orbit collisions and bifurcation curves

Periodic orbits in the SNM can undergo a particular form of bifurcation that occurs when the up and down periodic orbits of the same winding number meet on the symmetry line. These collisions were detected numerically in Refs. 12, 22 and 23. Further studies of this bifurcation can be found in Refs. 2 and 11.

From (4) it follows that, for a given a, only periodic orbits with $m/n<a$ exist at $b=0$. As the value of b increases, the up and down orbits approach each other, and at the bifurcation value, they collide and annihilate each other. For higher values of b, both orbits no longer exist. Figure 2 illustrates the behavior of periodic orbits as we increase b from $b=0$. Here the y-coordinates of the $m/n=3/8$ periodic orbits on s_1 are shown as a function of b for the fixed value of $a=0.4$.

Based on these numerical observations, the notion of a bifurcation curve in parameter space was defined in Ref. 12. The *m/n-bifurcation curve* $b=\Phi_{m/n}(a)$ is the set of (a,b) values for which the m/n up and down periodic orbits are at the point of collision. The main property of this curve is that

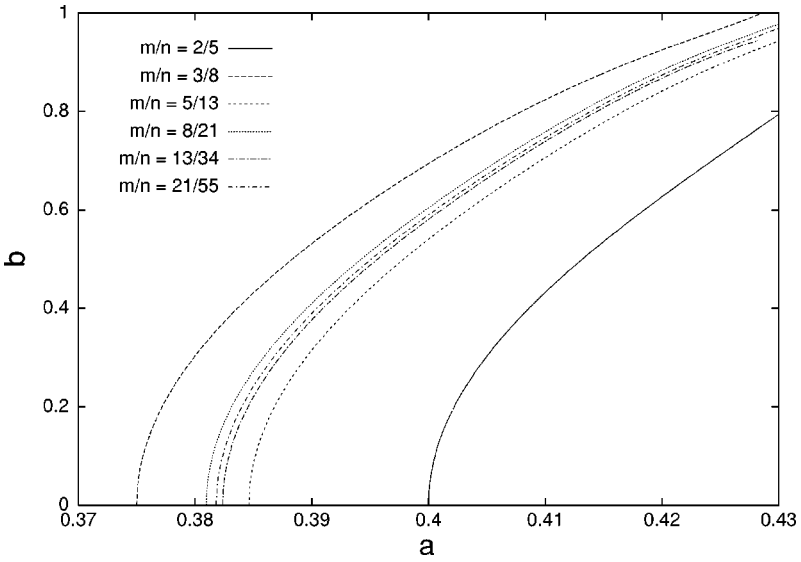

FIG. 3. Bifurcation curves for several convergents of $1/\gamma^2$.

for (a,b) values below $b=\Phi_{m/n}(a)$, the r/s periodic orbits, with $r/s<m/n$, exist. Thus, m/n is the maximum winding number for parameter values along the m/n-bifurcation curve.

The idea of approximating invariant tori with irrational winding numbers by periodic orbits is used to define the bifurcation curve for an invariant torus as follows:[12] The *ω-bifurcation curve* $b=\Phi_\omega(a)$ for an irrational ω is the set of (a,b) values such that $b=\Phi_\omega(a)=\lim_{i\to\infty}\Phi_{m_i/n_i}(a)$, where $\Phi_{m_i/n_i}(a)$ is the m_i/n_i-bifurcation curve and $\{m_i/n_i\}$ are the convergents of ω. For (a,b) points along the ω-bifurcation curve the invariant torus with irrational winding number ω is the curve of maximum winding number and is called *shearless*. Figure 3 depicts the bifurcation curves for several convergents of $1/\gamma^2$. This figure also makes it plausible that the limit in the above definition exists.

III. BREAKUP OF TORUS WITH $\omega=1/\gamma^2$

In this section, we present the analysis of the breakup of the shearless invariant torus in the standard nontwist map with winding number $\omega=1/\gamma^2$. Tables I and II list the convergents used for these calculations. For more details, see Ref. 24.

TABLE I. Some of the convergents of $\omega=[0,2,1,1,\ldots]$ for which the periodic orbits still exist at criticality.

$[i]$	F_i/F_{i+2}	$[i]$	F_i/F_{i+2}
[1]	1/3	[19]	6765/17711
[3]	3/8	[21]	17711/46368
[5]	8/21	[23]	46368/121393
[7]	21/55	[25]	121393/317811
[9]	55/144	[27]	317811/832040
[11]	144/377	[29]	832040/2178309
[13]	377/987	[31]	2178309/5702887
[15]	987/2584	[33]	5702887/14930352
[17]	2584/6765	[35]	14930352/39088169

A. Numerical methods

The computational steps necessary to find the critical point and the residue behavior of the approximating periodic orbits are as follows:

(1) Find a good approximation to the $1/\gamma^2$-bifurcation curve in (a,b)-space using the bifurcation curves for its convergents.
(2) Along this bifurcation curve, find the up and down periodic orbits on the symmetry line s_1 that approximate the invariant torus, and compute their residues.
(3) Locate the (a,b) point along the curve at which the residues exhibit critical behavior.
(4) Find the residues of the periodic orbits at criticality along the remaining symmetry lines.
(5) Find the eigenvalues of the unstable eigenmodes of the renormalization group operator. The details of how to do this depend crucially on the type of critical scaling behavior that is exhibited by the residues.

1. Searching for periodic orbits

Periodic orbits on the symmetry lines can be computed relatively easily for reversible maps using the following result:[12] If $(x,y)\in\Gamma_{0,1}$, then $M^n(x,y)=(x,y)$ if and only if $M^{n/2}(x,y)\in\Gamma_{0,1}$ (for n even) or $M^{(n\pm1)/2}(x,y)\in\Gamma_{1,0}$ (for n odd). Thus, for example, periodic orbits with odd period n on the s_1 symmetry line can be obtained by looking for points

TABLE II. Some of the convergents of $\omega=[0,2,1,1,\ldots]$ for which the periodic orbits do not exist at criticality.

$[i]$	F_i/F_{i+2}	$[i]$	F_i/F_{i+2}
[2]	2/5	[18]	4181/10946
[4]	5/13	[20]	10946/28657
[6]	13/34	[22]	28657/75025
[8]	34/89	[24]	75025/196418
[10]	89/233	[26]	196418/514229
[12]	233/610	[28]	514229/1346269
[14]	610/1597	[30]	1346269/3524578
[16]	1597/4181	[32]	3524578/9227465

on s_1 that are mapped to s_3 or s_4 after $(n+1)/2$ iterations. This can be implemented as a one-dimensional root finding problem by considering the zeros of the function $F(y) = \sin[2\pi(\hat{x} - a(1-\hat{y}^2)/2)]$, where $(\hat{x},\hat{y}) := M^{(n+1)/2}(0,y)$. The sine function is used to eliminate the difference between s_3 and s_4. Similar ideas can be applied to find other orbits.

2. Finding m/n-bifurcation curves

Recall that the bifurcation curve $\Phi_{m/n}(a)$ of a periodic orbit of winding number m/n was defined in Sec. II C to be the set of points (a,b), at which the up and down periodic orbits of winding number m/n collide along the s_1 symmetry line. Thus, at a given value of a, the function $F(y)$ has two roots for $b < \Phi_{m/n}(a)$, no roots (locally) for $b > \Phi_{m/n}(a)$ and a single root, which is also an extremum, for $b = \Phi_{m/n}(a)$. We thus search for the zero of the extremum of $F(y)$ as b is varied.

To find the whole (or large portions) of a bifurcation curve, we use the monotonic nature of the curve (see Fig. 3) as follows: Given a point (a_1,b_1) on the bifurcation curve, i.e., $b_1 = \Phi_{m/n}(a_1)$, we increase a by a fixed amount to $a_2 = a_1 + a_{\text{step}}$. We then start at the point (a_2,b_1) and increase b until we reach $b_2 = \Phi_{m/n}(a_2)$. To make sure that we are finding the correct bifurcation curve, we start searching (a,b)-space at $(a,b) = (m/n,0)$. Even then, the steps in a cannot be taken to be too large. Experience has shown that steps in a of 1×10^{-5} or 1×10^{-6} are safe. This method is unfortunately very slow because the part of the curve at small b values is very steep and the interesting (near critical) part of the curve is far away from the $b=0$ limit.

We managed to drastically improve the speed of these calculations by using the following ideas:

(1) Numerical evidence strongly suggests that a bifurcation curve is smooth and monotonically increasing, although it is not proved mathematically.[25] So we use linear extrapolation from two previous points to find the new value of b around which to search for the bifurcation point. It was found that any higher order extrapolation did not improve the algorithm further.
(2) To find bifurcation curves for periodic orbits with very large periods (e.g., of the order of several million) the following procedure is used: Starting at the bifurcation curve of a smaller period, we increase b until the bifurcation curve of the higher period is reached. The advantage of this procedure is that we do not need to do the extremely time consuming calculations of the bifurcation curves for very high period orbits starting at $b=0$, but rather we can search for them near the region of interest.

3. Finding $1/\gamma^2$-bifurcation curve

Recall that the $1/\gamma^2$-bifurcation curve was defined as the limit of m_i/n_i bifurcation curves, where m_i/n_i are convergents of $1/\gamma^2$. It was numerically observed that close to criticality, this limit is approached in accordance with the following scaling relation:[12]

$$\Phi_{[n+1]}(a) = \Phi_{1/\gamma^2}(a) + B_n(a)\,\nu_1^{n/12}, \tag{7}$$

where $\Phi_{[n]}(a)$ denotes the bifurcation curve of the periodic orbit with winding number $[n] = F_n/F_{n+2}$, ν_1 is a number to be determined later, and $B_n(a)$ is a period-twelve function, i.e., $B_{n+12}(a) = B_n(a)$.

If Eq. (7) holds, it follows that for fixed a

$$\Phi_{1/\gamma^2} = \lim_{n\to\infty} \frac{\Phi_{[n+1]}\Phi_{[n+12]} - \Phi_{[n]}\Phi_{[n+13]}}{(\Phi_{[n+1]} - \Phi_{[n]}) - (\Phi_{[n+13]} - \Phi_{[n+12]})}. \tag{8}$$

We obtained the $1/\gamma^2$-bifurcation curve using $n=19$ in Eq. (8), i.e., using the bifurcation curves for $[32]$, $[31]$, $[20]$ and $[19]$ (see Tables I and II).

Now one can justify *a posteriori* the use of Eq. (7). Solving Eq. (7) with $a = a_c$ for ν_1 yields

$$\nu_1 = \lim_{n\to\infty} \left(\frac{\Phi_{[n+13]}(a_c) - b_c}{\Phi_{[n+1]}(a_c) - b_c} \right), \tag{9}$$

and

$$B_n(a_c) = (\Phi_{[n+1]}(a_c) - b_c)\,\nu_1^{-n/12}, \tag{10}$$

where (a_c,b_c) is the critical point for breakup of the shearless $1/\gamma^2$ invariant torus, i.e., $b_c = \Phi_{1/\gamma^2}(a_c)$. We found that $\nu_1^{-1/12} = 2.678$. Some numerical evidence for the periodicity of $B_n(a_c)$ is given in Table III.

TABLE III. Period-12 behavior of the scaling function $B_n(a_c)$.

n	$B_n(a_c)$	n	$B_n(a_c)$
15	−0.4865	27	−0.4865
17	−0.7090	29	−0.7078
18	0.5019	20	0.5028
19	−0.3901	31	−0.3887

B. Results

In this subsection, we present the results of our computations.

1. Residue behavior at criticality

We computed bifurcation curves up to $[32] = 3524578/9227465$ and found the critical points along them, i.e., the parameter values along those curves for which the residues of approximating periodic orbits neither converge to zero nor diverge to infinity. Figure 4 shows the critical residue behavior of the up and down periodic orbits on the symmetry line s_1 along several different bifurcation curves. For lower period bifurcation curves, the residues first show signs of a six-cycle (to be discussed later in greater detail), but then converge to $|R_i| \approx 0.25$. This is because the invariant torus we are studying is not quite shearless. Thus we see the same behavior of the residues as in the case of a twist map. As we proceed to higher period bifurcation curves, the behavior of the residues of the approximating periodic orbits found along the s_1 symmetry line resembles more and more a six-cycle. A renormalization group interpretation of these results is given in Sec. IV.

Finally, we found the critical point (a_c,b_c) along the $1/\gamma^2$-bifurcation curve to be the following:

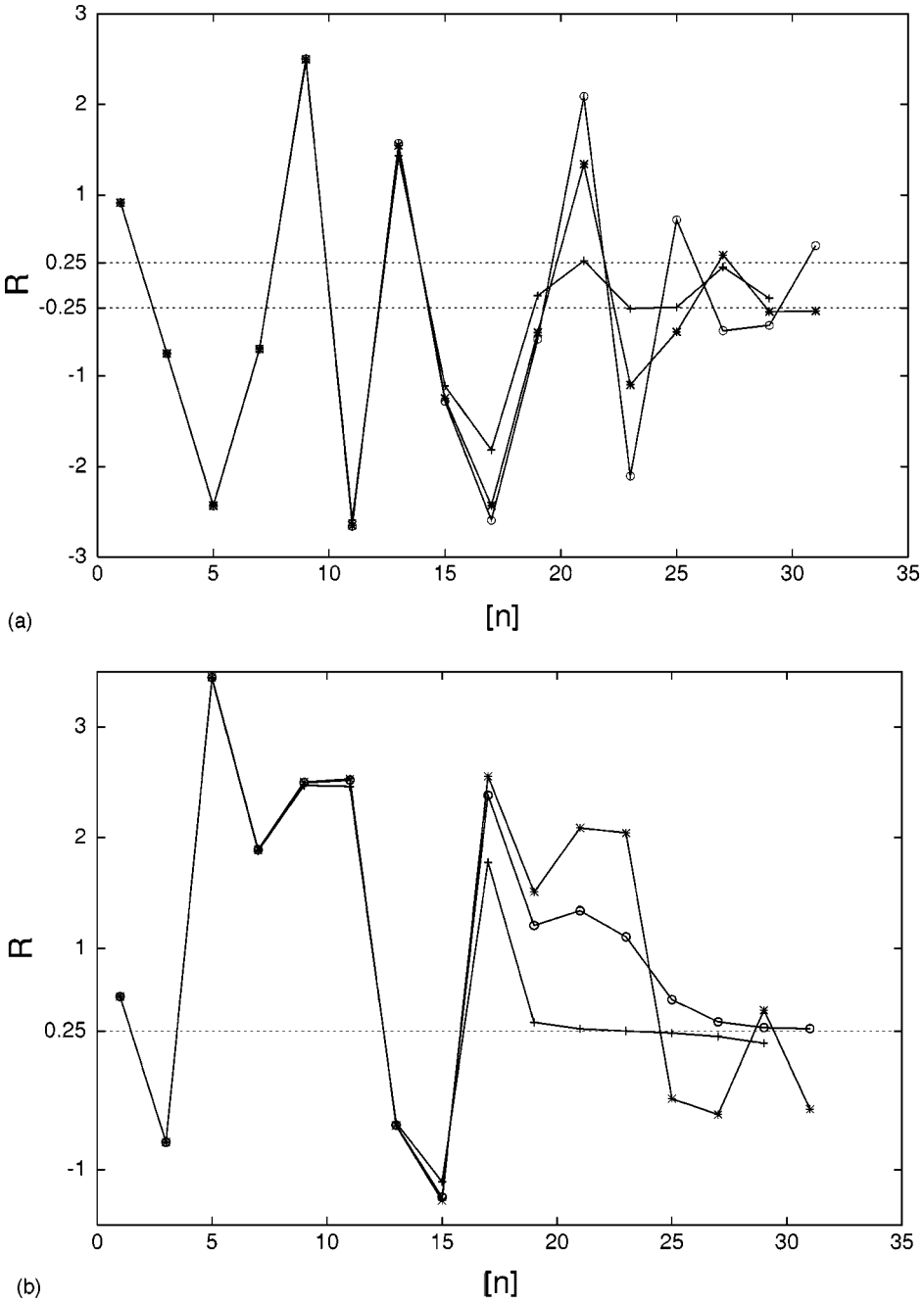

FIG. 4. Residue behavior of the up (top figure) and down (bottom figure) periodic orbits on s_1 at the critical points on bifurcation curves of [20] (+), [24] (○) and [28] (*).

$$a_c = 0.425160543, \quad b_c = 0.9244636470355. \tag{11}$$

At the critical parameter values (a_c, b_c), the residues of the down periodic orbits on s_1, which are equal to the residues of the up periodic orbits on s_2 because of the symmetry of the map [see Eq. (6)], converge to the six-cycle[26] $\{C_1, C_2, C_3, C_4, C_5, C_6\}$, where

$$\begin{aligned} C_1 &= -0.609 \pm 0.005, & C_2 &= -1.288 \pm 0.002, \\ C_3 &= 2.593 \pm 0.005, & C_4 &= 1.584 \pm 0.008, \\ C_5 &= 2.336 \pm 0.006, & C_6 &= 2.593 \pm 0.005. \end{aligned} \tag{12}$$

The six-cycle can clearly be seen in Fig. 5 which shows the residues of the up and down periodic orbits at the critical point along the s_1 symmetry line. The residues of the up periodic orbits on s_1 (and of the down periodic orbits on s_2) converge to the six-cycle $\{D_1, D_2, D_3, D_4, D_5, D_6\}$, where

$$\begin{aligned} D_1 &= 1.584 \pm 0.008, & D_2 &= -1.288 \pm 0.002, \\ D_3 &= -2.630 \pm 0.006, & D_4 &= -0.609 \pm 0.005, \\ D_5 &= 2.336 \pm 0.006, & D_6 &= -2.630 \pm 0.006. \end{aligned} \tag{13}$$

The residue convergence for other symmetry lines is shown in Table IV where we denote by R_{u_i} and R_{d_i} the residues of the up and down periodic orbit on the symmetry line s_i. Note that the six-cycle $\{D_i\}$ of R_{u_1} and R_{d_2} (respectively, the six-cycle $\{C_i\}$ of R_{u_2} and R_{d_1}) is observed to be the same as that of R_{u_3} and R_{d_4} (respectively, R_{u_4} and R_{d_3}) except it is shifted. The two six-cycles are related because of the sym-

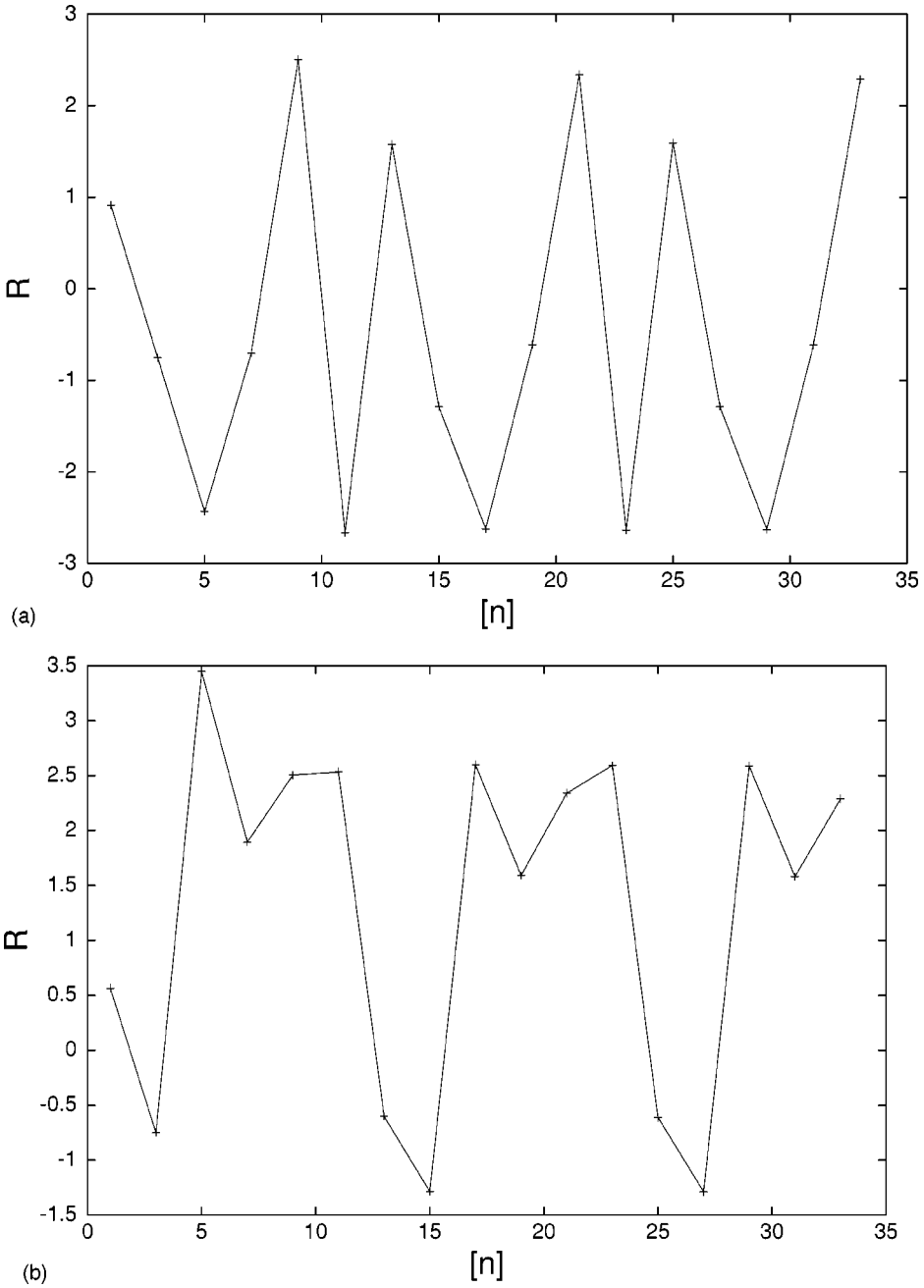

FIG. 5. Residue behavior of the up (left figure) and down (right figure) periodic orbits on s_1 at the critical point on $1/\gamma^2$-bifurcation curve.

metry of the map as follows: $D_1=C_4$, $D_2=C_2$, $D_4=C_1$, $D_5=C_5$, $C_3=C_6$, and $D_3=D_6$. It was numerically observed that $C_6\approx -D_6$, and therefore $C_3\approx -D_3$. Using these relations we see that there are only five independent residues which we take to be C_1, C_2, C_3, C_4, and C_5.

TABLE IV. Period-six convergence pattern of the residues near criticality along the different symmetry lines.

$[i]$	$R_{u_1}=R_{d_2}$	$R_{u_2}=R_{d_1}$	$R_{u_3}=R_{d_4}$	$R_{u_4}=R_{d_3}$
[1] , [13] , [25]	D_1	C_1	D_4	C_4
[3] , [15] , [27]	D_2	C_2	D_5	C_5
[5] , [17] , [29]	D_3	C_3	D_6	C_6
[7] , [19] , [31]	D_4	C_4	D_1	C_1
[9] , [21] , [33]	D_5	C_5	D_2	C_2
[11] , [23] , [35]	D_6	C_6	D_3	C_3

We compared the values of the residues at three different points along the $1/\gamma^2$-bifurcation curve, one point below criticality, one at criticality, and one above criticality: $(a_-,b_-)=(0.425160540,0.9244636195728)$, $(a_c,b_c)=(0.425160543,0.9244636470355)$ and $(a_+,b_+)=(0.425160545,0.9244636653440)$, respectively. The numerical results for the C_i are listed in Table V. We see that each element of the six-cycle tends to zero for (a_-,b_-), to infinity for (a_+,b_+), while it tends to the critical value at (a_c,b_c). Figure 6 clearly illustrates this behavior.

A comparison with the results of Ref. 12 shows that, within numerical accuracy, we found the same values for the residues of the six-cycle, but the sequence has shifted by two: $C_1=H_3$, $C_2=H_4$, $C_3=H_5$, $C_4=H_6$, $C_5=H_1$ and $C_6=H_2$, where H_i denote the residues for the $1/\gamma$ case

TABLE V. Numerical values of the residue six-cycle C_i at $z_-=(a_-,b_-)$, $z_c=(a_c,b_c)$, and $z_+=(a_+,b_+)$.

[n]		z_-	z_c	z_+		z_-	z_c	z_+
[01]	C_1	0.565	0.565	0.565	C_4	0.914	0.914	0.914
[07]		−0.702	−0.702	−0.702		1.893	1.893	1.893
[13]		−0.601	−0.601	−0.601		1.574	1.574	1.574
[19]		−0.611	−0.611	−0.612		1.590	1.591	1.592
[25]		−0.610	−0.612	−0.614		1.578	1.591	1.599
[31]		−0.566	−0.612	−0.644		1.406	1.581	1.710
[03]	C_2	−0.752	−0.752	−0.752	C_5	2.169	2.169	2.169
[09]		−1.328	−1.328	−1.328		2.505	2.505	2.505
[15]		−1.286	−1.286	−1.286		2.329	2.329	2.329
[21]		−1.289	−1.290	−1.291		2.337	2.340	2.341
[27]		−1.273	−1.289	−1.300		2.300	2.338	2.364
[33]		−1.161	−1.249	−1.276		1.873	2.288	2.614
[05]	C_3	3.450	3.450	3.450	C_6	3.450	3.450	3.450
[11]		2.534	2.534	2.534		2.534	2.534	2.534
[17]		2.598	2.598	2.598		2.598	2.598	2.598
[23]		2.588	2.594	2.598		2.588	2.594	2.598
[29]		2.498	2.588	2.650		2.498	2.588	2.650

found in Ref. 12. A similar shift by two occurs for other symmetry lines.

2. Spatial scaling at criticality

As expected, the shearless curve exhibits scale invariance at criticality, which can be demonstrated explicitly by using *symmetry line coordinates*[12] $(\hat{x},\hat{y})$ defined by $\hat{x}=x-a(1-y^2)/2$ and $\hat{y}=y-y_s$. In these coordinates, the s_3 symmetry line becomes a straight line that intersects the shearless curve at the origin. We find that, in symmetry line coordinates, the shearless $1/\gamma^2$ invariant torus at criticality remains invariant under a scale change $(x,y)\rightarrow(\alpha^{12}x,\beta^{12}y)$. This property is illustrated in Fig. 7.

As described in Ref. 13, we can find y_s using

$$y_s=\lim_{i\rightarrow\infty}\frac{y_{[2i+1]}\ \ y_{[2i+11]}-y_{[2i-1]}\ \ y_{[2i+13]}}{(y_{[2i+1]}-y_{[2i-1]})-(y_{[2i+13]}-y_{[2i+11]})}$$
$$\approx 0.47253494777, \tag{14}$$

where $y_{[n]}$ denotes the y-coordinate of the periodic orbit $[n]$ along the s_3 symmetry line. To obtain the quoted value of y_s we used $i=10$. We then obtained α and β as follows:[27]

$$\alpha=\lim_{n\rightarrow\infty}\left|\frac{\hat{x}_{[2i+1]}}{\hat{x}_{[2i+13]}}\right|^{1/12}\approx 1.61759 \tag{15}$$

and

$$\beta=\lim_{n\rightarrow\infty}\left|\frac{\hat{y}_{[2i+1]}}{\hat{y}_{[2i+13]}}\right|^{1/12}\approx 1.65702, \tag{16}$$

where $(\hat{x}_{[n]},\hat{y}_{[n]})$ are symmetry line coordinates of the point of the periodic orbit $[n]$ that is the closest to the origin. Within numerical accuracy, these values are the same as in Ref. 13.

Further numerical analysis shows that periodic orbits also exhibit scaling behavior locally near the s_3 symmetry line. Figure 8 shows points of the periodic orbit $[n]=[21]$ (in symmetry line coordinates) and points of the periodic orbit [33] with the x and y coordinates rescaled by α^{12} and β^{12}, respectively. The result suggests that periodic orbits remain invariant under a simultaneous spatial rescaling and shifting of the winding number by twelve from $[n]$ to $[n+12]$.

C. Numerical accuracy

We conclude this section with comments about the numerical accuracy of the results.

(1) Points on the m/n-bifurcation curves were found with an accuracy ranging between 10^{-12} and 10^{-15}, where the larger value corresponds to larger periods. We obtain this measure of accuracy from the condition

$$F(y)=0,\quad F'(y)=0,\quad \text{and}\quad F''(y)\neq 0, \tag{17}$$

as explained previously. The numbers quoted above are the values of $F(y)$ obtained at the numerically found minima in y.

(2) Periodic orbits along the different symmetry lines around the critical point were found with an accuracy ranging between 10^{-15} and 10^{-17}. Here, the criterion is the difference between the winding number m/n of the periodic orbit of interest, and the winding number of the orbit that results when starting at the numerically found location of the periodic orbit on the respective symmetry line, and then iterating the map.

(3) A criterion for the accuracy of the scaled bifurcation curve Φ_{1/γ^2} is harder to find, since the location of the actual curve is unknown. An upper bound on the error, though, should be the distance between the Φ_{1/γ^2} and $\Phi_{[37]}$, since the latter definitely lies on the other side of Φ_{1/γ^2}. This error was found to be approximately 2×10^{-13}.

(4) A criterion for the accuracy of the critical point in parameter space, (a_c,b_c) is even harder to define, since we cannot actually find the residues of existing orbits of *all* periods, which is required to check if the six-cycle at that point continues *ad infinitum*. We believe that the value for a_c is accurate up to 1×10^{-9}.

(5) The uncertainties for the critical residues, quoted above in Eq. (12), were computed from the variation in numerical values of residues at a_c for the three or four highest period orbits found (e.g., for C_1, using residues of [13], [19], [25] and [31]).

(6) If we evaluate the residues of the up and down periodic orbits along the s_1 and s_3 symmetry lines, then the residues on the other two symmetry lines can be constructed using symmetry arguments (see Sec. II A). But, as a check of the numerical procedures, we independently evaluated the residues on all the four symmetry lines and confirmed the symmetry arguments.

IV. RENORMALIZATION GROUP INTERPRETATION

In this section, we interpret the above results within the renormalization group framework. The analysis follows Ref.

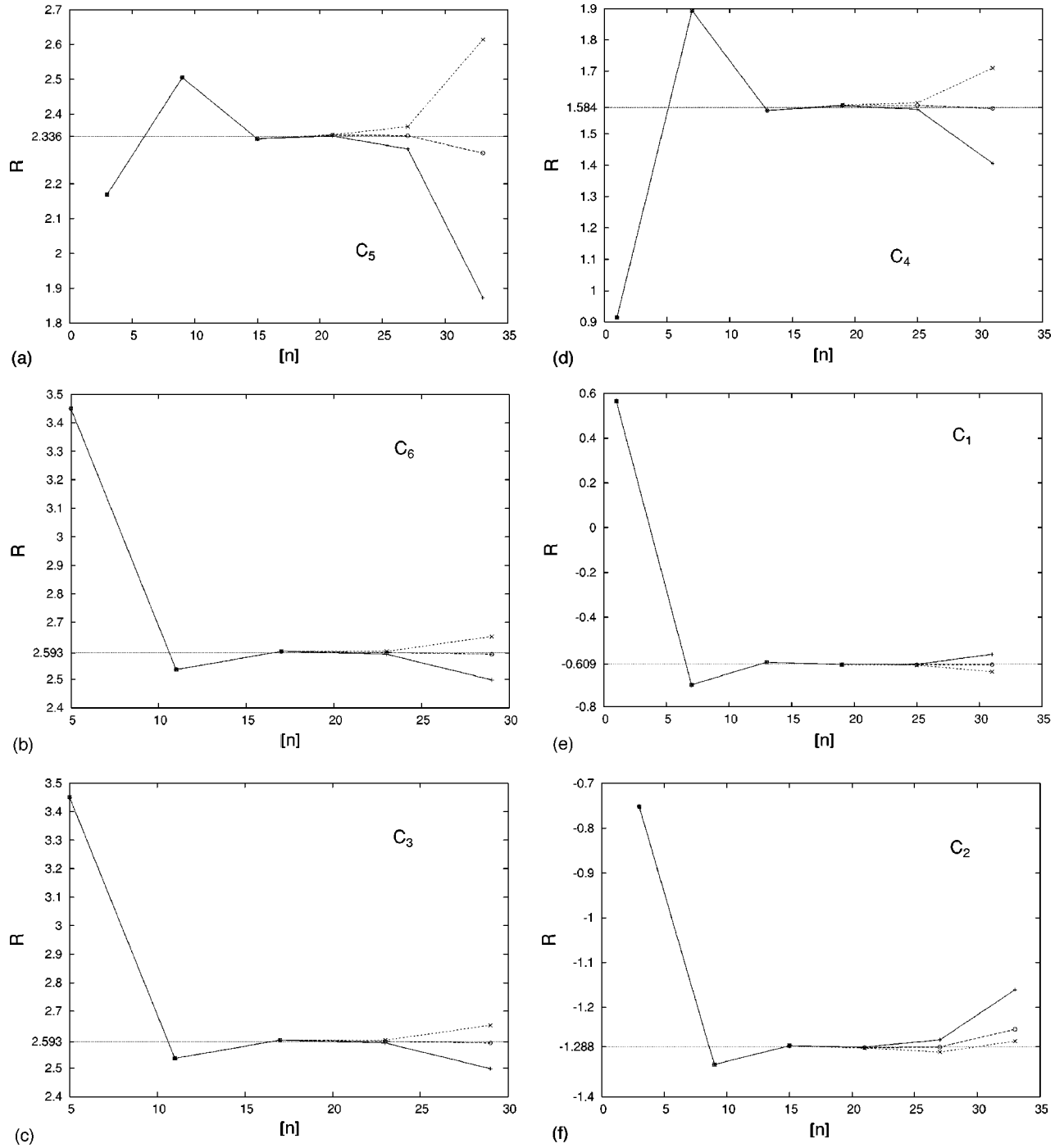

FIG. 6. Residue convergence for C_1 through C_6 at z_1 (+), z_2 (○) and z_3 (×) (see Table V).

13 closely, since, as expected, the residue behavior exhibits a six-cycle at criticality. But, because of the different winding number (i.e., different from $1/\gamma$) the renormalization group operator will have a different form.

Renormalization ideas have been used fruitfully in area-preserving maps and Hamiltonian flows. (See, e.g., Refs. 28–34 and references therein.) In contrast to mathematical KAM theory, which proves the existence of dense sets of invariant tori in regions of phase space, the renormalization group approach addresses the problem of the destruction of an invariant torus with a *specific* winding number under strong perturbation.

The following renormalization approach (see e.g., Refs. 13 and 35) is based on the residue criterion (Sec. II A). To study the breakup of an invariant torus of winding number ω, we loosely represent the map M as

$$M=(R_1,R_2,R_3,\ldots), \tag{18}$$

where the $\{R_i\}$ are the residues of the periodic orbits with-winding numbers $\{m_i/n_i\}$, the convergents of ω. For ex-

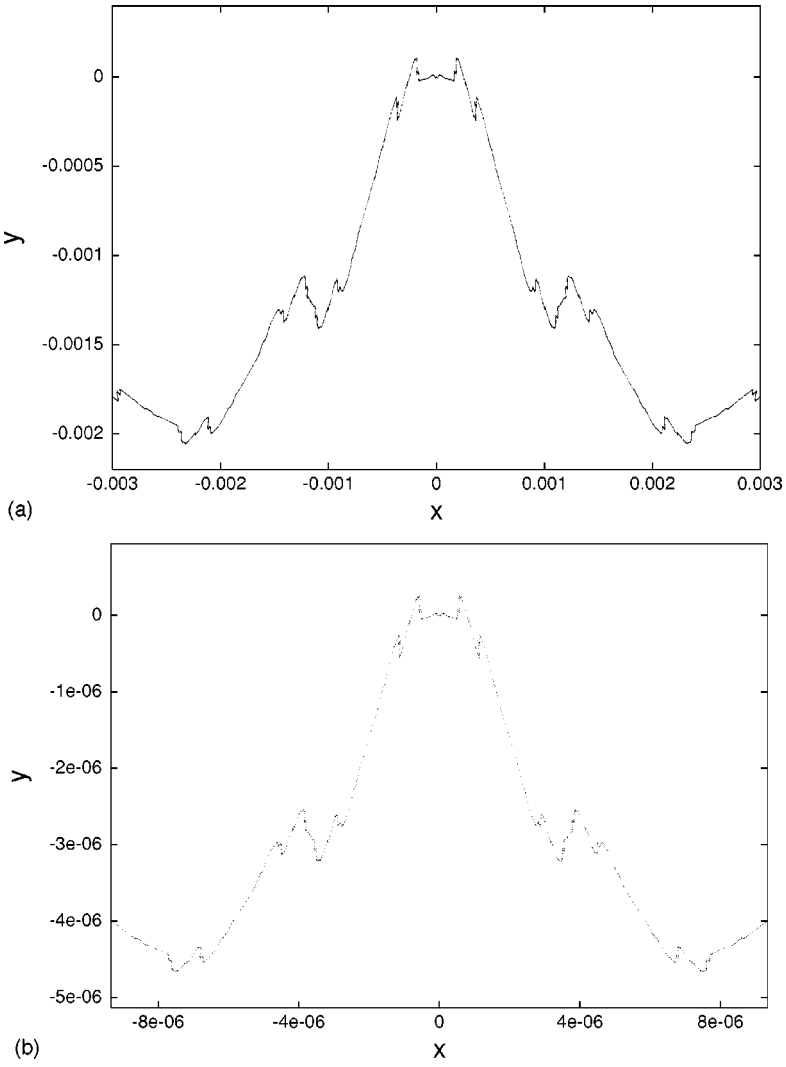

FIG. 7. Invariance under rescaling of shearless $1/\gamma^2$ torus at criticality.

ample, the integrable map will be represented by $(0,0,0,\ldots)$ because all the orbits are parabolic in that case. The key idea is to construct an operator $\mathcal{R}$ that explores the infinite tail of (18) by mapping a map given by (18) to another map, $\mathcal{R}(M)$, represented by $\mathcal{R}(M)=(\hat{R}_1,\hat{R}_2,\ldots,\hat{R}_i,\ldots)$, where $\hat{R}_i=R_{i+1}$. This operation can be interpreted as a *time renormalization* since periodic orbits with large periods are transformed into periodic orbits with smaller periods.

The residue criterion can now be rephrased in this framework:

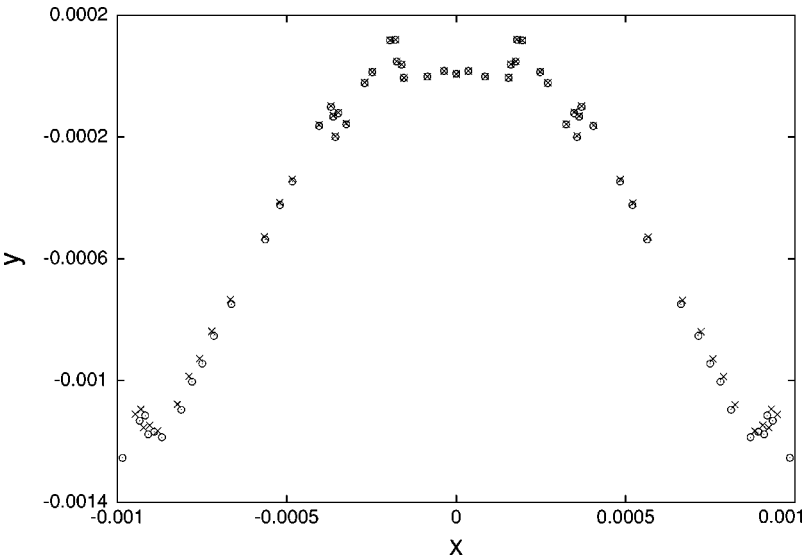

FIG. 8. Invariance of periodic orbits under simultaneous rescaling and shift of winding numbers by twelve. Here we show the periodic orbits [21] ($\times$) and [33] ($\bigcirc$) after rescaling of x and y coordinates by α^{12} and β^{12}, respectively.

(1) If $\lim_{n\to\infty}\mathcal{R}^n(M)=(0,0,0,\ldots)$, the invariant torus exists.
(2) If $\lim_{n\to\infty}\mathcal{R}^n(M)=(\pm\infty,\pm\infty,\ldots)$, the invariant torus is destroyed.
(3) If $\lim_{n\to\infty}\mathcal{R}^n(M)$ is a map for which the residues have finite, nonzero values, i.e., a map that is invariant under the action of $\mathcal{R}^m$ (a fixed point of $\mathcal{R}^m$) for some $m>0$, the invariant torus is at the threshold of destruction. Possible scenarios are the convergence of the residues to a fixed value or to a convergent subsequence.

There are two kinds of fixed points: *simple* fixed points and *critical* fixed points. In the case of area-preserving maps, we come to the following interpretation. A *simple* fixed point is an integrable map (all the residues are zero), and its basin of attraction contains all the maps for which the invariant torus exists. A *critical* fixed point is a map for which the invariant torus under consideration is at criticality. All the maps in its basin of attraction exhibit the same universal behavior at the critical breakup.

A. Renormalization group operator

Following the discussion in Refs. 33 and 13, we use pairs of commuting maps because they provide a simple way to define the renormalization operators for invariant tori.

A *pair of commuting maps* is an ordered pair of maps, (U,T), such that $UT=TU$. An *orbit* of a point (x,y) generated by (U,T) is the set of points $\{U^mT^n(x,y)\}$, where m and n are integers. A *periodic orbit of period* m/n is an orbit for which $U^mT^n(x_i,y_i)=(x_i,y_i)$.

For the breakup of the invariant torus with winding number $\omega=1/\gamma^2$, we define the renormalization group operator by

$$\mathcal{R}\begin{pmatrix}U\\T\end{pmatrix}:=B\begin{pmatrix}U^{-1}T^{-1}\\ U\quad T^2\end{pmatrix}B^{-1}. \tag{19}$$

As for the case of $1/\gamma$,[13] this operator contains both time and space renormalization as follows:

The *space renormalization* is represented by the operator B, which rescales the (x,y) coordinates, i.e., $(x,y)\to B(x,y)$ where

$$B=\begin{pmatrix}r & 0\\ 0 & s\end{pmatrix}. \tag{20}$$

At the critical fixed point studied in this article, we see that $r=\alpha$ and $s=\beta$ given by Eqs. (15) and (16).

The *time renormalization* is, again, accomplished by the specific combination of the commuting maps. If (x,y) is a periodic orbit of (U,T) with winding number F_i/F_{i+2}, then $B(x,y)$ is a periodic orbit of $(\hat{U},\hat{T})=\mathcal{R}(U,T)$ with winding number F_{i-1}/F_{i+1}, as can be verified as follows:

$$\begin{aligned}\hat{U}^{F_{i-1}}\ \hat{T}^{F_{i+1}}B(x,y)&=B(UT)^{-F_{i-1}}\ (UT^2)^{F_{i+1}}(x,y)\\&=BU^{-F_{i-1}+F_{i+1}}\ T^{-F_{i-1}+2F_{i+1}}(x,y)\\&=BU^{F_i}\ T^{F_{i+2}}(x,y)=B(x,y).\end{aligned}$$

By induction, an orbit with winding number F_i/F_{i+2} under (U,T) is transformed into an orbit of $\mathcal{R}^n(U,T)$ with winding number F_{i-n}/F_{i+2-n}.

B. Simple periodic orbit of $\mathcal{R}$

We can find the integrable period-two orbit $(U_\pm,T_\pm)$ of the renormalization operator (19) by requiring that $\mathcal{R}(U_\pm,T_\pm)=(U_\mp,T_\mp)$. This two-cycle is given by the following pairs of maps:

$$U_\pm\begin{pmatrix}x\\y\end{pmatrix}=\begin{pmatrix}x-\gamma^2\mp y^2/\gamma^2\\ y\end{pmatrix},\quad T_\pm\begin{pmatrix}x\\y\end{pmatrix}=\begin{pmatrix}x+1\pm y^2\\ y\end{pmatrix}, \tag{21}$$

where the rescaling of the coordinates is given by

$$B=\begin{pmatrix}-\gamma & 0\\ 0 & \pm\gamma\end{pmatrix}. \tag{22}$$

Using the definition $U_\pm^mT_\pm^n(x,y)=(x,y)$ of the periodic orbits of period m/n, we get the rotation number as a function of y:

$$\begin{aligned}\omega_\pm(y)&=-\frac{1\pm y^2}{-\gamma^2\mp y^2/\gamma^2}=\frac{1}{\gamma^2}(1\pm y^2)\left(1\pm\frac{y^2}{\gamma^4}\right)^{-1}\\&\approx\frac{1}{\gamma^2}\left[1\pm\left(1-\frac{1}{\gamma^4}\right)y^2+\ldots\right].\end{aligned}$$

Thus we see that the map (U_-,T_-) is locally equivalent, under a change of coordinates, to the SNM with parameters $(a,b)=(1/\gamma^2,0)$.

C. Critical periodic orbit of $\mathcal{R}$

The next step is to analyze the critical periodic orbit of $\mathcal{R}$. Consider the nontwist map

$$\begin{aligned}\mathcal{C}=(&C_1,-,C_2,-,C_3,-,C_4,-,C_5,\\&-,C_6,-,C_1,-,C_2,\ldots),\end{aligned} \tag{23}$$

where the C_i are the elements of the six-cycle computed earlier, and the "$-$" denote the periodic orbits that do not exist (see Table II). By construction, this map is a period-12 orbit of the renormalization group operator (a fixed point of $\mathcal{R}^{12}$), i.e.,

$$\mathcal{R}^{12}\mathcal{C}=\mathcal{C}. \tag{24}$$

In Sec. III B, we found that the residues of the periodic orbits approximating the $1/\gamma^2$-shearless curve in the standard nontwist map exhibit convergence to the six-cycle $\{C_i\}$. Assuming that we can fine-tune the results for (a_c,b_c), we expect that $\lim_{n\to\infty}\mathcal{R}^nM(a_c,b_c)=\mathcal{C}$.

If we are studying the breakup of the $1/\gamma^2$-shearless curve for parameter values along the bifurcation curve for one of the low-period convergents, then we start near the stable manifold of the critical periodic orbit of $\mathcal{R}$. But, under the action of $\mathcal{R}$, we are pushed along an unstable direction. Thus, we see parts of the six-cycle of residues (see Fig. 4), but the limiting residue behavior is observed to be $\lim_{i\to\infty}|R_i|\approx 0.25$, which is characteristic for the critical fixed point of *twist* maps (see, e.g., Ref. 33). In renormaliza-

tion group language, this means that part of the unstable manifold of the critical nontwist fixed point [maps for which (a,b) is below (a_c,b_c)] is in the basin of attraction of the critical twist fixed point.

D. Eigenvalues

As shown in Ref. 13, it is possible to use our numerical data to draw further conclusions about the renormalization group operator $\mathcal{R}$, in particular to compute its unstable eigenvalues. The main difficulty in computing these eigenvalues is that the space of maps is infinite-dimensional whereas the (a,b) parameter space has only two dimensions. But the fact that we can find an isolated point (a_c,b_c) in parameter space at which the map is at criticality means that the dimension of the unstable manifold is two. The map M at (a_c,b_c) is the intersection point of the two-parameter family of maps with the stable manifold of the fixed point, i.e., values a_c and b_c describe the location of the critical fixed point of $\mathcal{R}$ [12] in its unstable manifold.

Below, we first compute the eigenvalues characterizing the approach to (a_c,b_c) in the (a,b) parameter space using the numerical results from above. As shown in Ref. 13, based on the type of numerical data obtained, the two eigenvalues can be found by

$$\nu_1=\lim_{n\to\infty}\left(\frac{\Phi_{[n+12]}(a_c)-b_c}{\Phi_{[n]}(a_c)-b_c}\right) \tag{25}$$

and

$$\nu_2=\lim_{n\to\infty}\left(\frac{a_{c\,[2n+12]}-a_c}{a_{c\,[2n]}-a_c}\right). \tag{26}$$

The last step is to relate the values ν_i to the unstable eigenvalues δ_i of the renormalization group operator $\mathcal{R}$. The key idea is to study the behavior of the residues of the periodic orbits approximating ω at the (a,b) values used in the computation of ν_i. For details see Ref. 13.

Denoting the unstable eigenvalues of $\mathcal{R}$ by δ_1 and δ_2, we conclude that $\delta_i=(1/\nu_i)^{1/12}$. We find numerical values of

$$\delta_1\approx 2.678, \quad \delta_2\approx 1.583. \tag{27}$$

Comparing these to the values found in Ref. 13 shows that within (assumed) numerical uncertainty these values are the same as those for $1/\gamma$, as predicted. The a_c values used to determine δ_2 were $a_{c[26]}$ and $a_{c[14]}$, which explains the larger discrepancy. Work is under way to improve this result.

V. CONCLUSION

We have shown through numerical simulations that the critical residue values at the breakup of the $1/\gamma^2$-shearless curve in the standard nontwist map coincide with those of the $1/\gamma$-shearless curve. In addition, the critical scaling parameters and the unstable eigenvalues of the renormalization group operator were found to be the same for both cases. The main differences are the location of the respective critical point in parameter space and the detailed form of the renormalization group operator in terms of commuting maps pairs.

Future work includes the search for the breakup values of more winding numbers to map out the details of the critical function depicted in Fig. 1. In addition, new fixed points of the renormalization group operator might be obtained by studying the breakup of shearless curves with non-noble winding numbers.

ACKNOWLEDGMENTS

The authors would like to thank John Greene and Diego del-Castillo-Negrete for many helpful discussions. This research was supported in part by U.S. Department of Energy Contract No. DE-FG01-96ER-54346 and by an appointment of A. Wurm to the U.S. Department of Energy Fusion Energy Postdoctoral Research Program administered by the Oak Ridge Institute for Science and Education.

[1] D. del-Castillo-Negrete and P. J. Morrison, "Chaotic transport by Rossby waves in shear flow," Phys. Fluids A **5**, 948 (1993).
[2] E. Petrisor, "Nontwist area preserving maps with reversing symmetry group," Int. J. Bifurcation Chaos Appl. Sci. Eng. **11**, 497 (2001).
[3] R. Balescu, "Hamiltonian nontwist maps for magnetic field lines with locally reversed shear in toroidal geometry," Phys. Rev. E **58**, 3781 (1998).
[4] W. Horton, H.-B. Park, J.-M. Kwon, D. Strozzi, P. J. Morrison, and D.-I. Choi, "Drift wave test particle transport in reversed shear profile," Phys. Plasmas **5**, 3910 (1998).
[5] W. T. Kyner, "Rigorous and formal stability of orbits about an oblate planet," Mem. Am. Math. Soc. **81**, 1 (1968).
[6] C. Chandre, D. Farrelly, and T. Uzer, "Threshold to chaos and ionization for the hydrogen atom in rotating fields," Phys. Rev. A **65**, 053402 (2002).
[7] H. R. Dullin, J. D. Meiss, and D. Sterling, "Generic twistless bifurcations," Nonlinearity **13**, 202 (2000).
[8] J. P. Van Der Weele, T. P. Valkering, H. W. Capel, and T. Post, "The birth of twin Poincaré–Birkhoff chains near 1:3 resonance," Physica A **153**, 283 (1988); J. P. Van Der Weele and T. P. Valkering, "The birth process of periodic orbits in non-twist maps," *ibid.* **169**, 42 (1990).
[9] A. Delshams and R. de la Llave, "KAM theory and a partial justification of Greene's criterion for non-twist maps," SIAM (Soc. Ind. Appl. Math.) J. Math. Anal. **31**, 1235 (2000).
[10] J. Franks and P. Le Calvez, "Regions of instability for nontwist maps," preprint, math.DS/9910152, Los Alamos (1999).
[11] C. Simó, "Invariant curves of analytic perturbed nontwist area preserving maps," Regular and Chaotic Dyn. **3**, 180 (1998).
[12] D. del-Castillo-Negrete, J. M. Greene, and P. J. Morrison, "Area preserving nontwist maps: Periodic orbits and transition to chaos," Physica D **91**, 1 (1996).
[13] D. del-Castillo-Negrete, J. M. Greene, and P. J. Morrison, "Renormalization and transition to chaos in area preserving nontwist maps," Physica D **100**, 311 (1997).
[14] S. Shinohara and Y. Aizawa, "The breakup condition of shearless KAM curves in the quadratic map," Prog. Theor. Phys. **97**, 379 (1997).
[15] Note, that the map used in Ref. 14 is different from the map we use [Eq. (1)], but they are related by a coordinate transformation, including rescaling of parameters.
[16] J. Stark, "Determining he critical transition for circles of arbitrary rotation number," Phys. Lett. A **163**, 258 (1992).
[17] J. M. Greene, "A method for computing the stochastic transition," J. Math. Phys. **20**, 1183 (1979).
[18] A. Ya. Khinchin, *Continued Fractions*, 3rd ed. (University of Chicago Press, Chicago, IL, 1964).
[19] C. Falcolini and R. de la Llave, "A rigorous partial justification of Greene's residue criterion," J. Stat. Phys. **67**, 609 (1992).
[20] R. S. MacKay, "On Greene's residue criterion," Nonlinearity **5**, 161 (1992).
[21] R. de Vogelaere, "On the structure of symmetric periodic solutions of conservative systems, with applications," in *Contributions to the Theory of Nonlinear Oscillations*, Vol. IV, edited by S. Lefschetz (Princeton University Press, Princeton, NJ, 1958), p. 53.
[22] J. E. Howard and S. M. Hohs, "Stochasticity and reconnection in Hamil-

tonian systems,'' Phys. Rev. A **29**, 418 (1984); J. E. Howard and J. Humphreys, ''Nonmonotonic twist maps,'' Physica D **80**, 256 (1995).
[23] T. H. Stix, ''Current penetration and plasma disruption,'' Phys. Rev. Lett. **36**, 521 (1976).
[24] A. Wurm, ''Renormalization group applications in area-preserving nontwist maps and relativistic quantum field theory,'' Ph.D. thesis, The University of Texas at Austin, Austin, May 2002.
[25] There is a proof for the existence of smooth bifurcation curves for small values of *b* (Ref. 9).
[26] For comments about the numerical accuracy see Sec. III C.
[27] Note that these equations are derived *assuming* that the shearless curve scales at criticality. The validity of this assumption is demonstrated *a posteriori* by Fig. 7.
[28] J. J. Abad and H. Koch, ''A renormalization group for Hamiltonians: Numerical results,'' Nonlinearity **11**, 1185 (1998); ''Renormalization and periodic orbits for Hamiltonian flows,'' Commun. Math. Phys. **212**, 371 (2000).
[29] C. Chandre and H. R. Jauslin, ''Renormalization-group analysis for the transition to chaos in Hamiltonian systems,'' Phys. Rep. **365**, 1 (2002).
[30] D. F. Escande and F. Doveil, ''Renormalization method for computing the threshold of the large-scale stochastic instability in two degrees of freedom Hamiltonian systems,'' J. Stat. Phys. **26**, 257 (1981).
[31] J. M. Greene, ''How a swing behaves,'' Physica D **18**, 427 (1986).
[32] H. Koch, ''A renormalization group for Hamiltonians, with applications to KAM tori,'' Ergod. Theory Dyn. Syst. **19**, 475 (1999); ''A renormalization group fixed point associated with the breakup of golden invariant tori,'' mp_arc 02-175, April 9, 2002.
[33] R. S. MacKay, ''Renormalization in area preserving maps,'' Ph.D. thesis, Princeton University, 1982; ''A renormalization approach to invariant circles in area-preserving maps,'' Physica D **7**, 283 (1983).
[34] S. J. Shenker and L. P. Kadanoff, ''Critical behavior of a KAM surface: I. Empirical results,'' J. Stat. Phys. **27**, 631 (1982).
[35] J. M. Greene, ''The status of KAM theory from a physicist's point of view,'' in *Chaos in Australia*, edited by G. Brown and A. Opie (World Scientific, Singapore, 1993), p. 8.